Regulation of syntaxin1A–munc18 complex for SNARE pairing in HEK293 cells

Svetlana E. Gladycheva, Chi S. Ho, Yue Ying F. Lee and Edward L. Stuenkel

Department of Molecular and Integrative Physiology, University of Michigan, Ann Arbor, MI 48109, USA

The formation and dissolution of SNARE protein complexes is essential for Ca^{2+}-triggered fusion of neurotransmitter-filled vesicles at the presynaptic membrane. Among the pre-synaptic SNARE proteins, the activation of the Q-SNARE syntaxin1A is a critical event for SNARE complex formation. Activation requires syntaxin1A to transit from a munc18-bound non-interacting state to one competent for SNARE binding. The molecular mechanisms that regulate this transition remain unclear. The propensity of syntaxin1A to promote voltage-dependent steady-state inactivation of N-type Ca^{2+} channels and accelerate their entry into inactivation was used in a heterologous cell expression system to elucidate regulation of syntaxin1A protein–protein interactions. We report that coexpression of munc18 eliminated the promoting effect of syntaxin1A on inactivation. This effect of munc18 was completely disrupted by coexpression of munc13-1, but not munc13-2 or munc13-3. Also, since expression of munc13-1 with syntaxin1A resulted in an inactivation phenotype identical to that of munc18 with syntaxin1A, the action of munc13-1 on the munc18–syntaxin1A complex was functionally unique and did not result from competitive binding interactions. Furthermore, munc13 expressed with syntaxin1A and munc18 promoted redistribution of a cytosolic SNAP25 mutant to the membrane, a result indicative of syntaxin1A–SNAP25 SNARE pairing. These data demonstrate an important role of munc13 to control the protein–protein interactions of syntaxin1A *in vivo,* and support munc13 as critical to dissociating syntaxin1A–munc18 complexes and making syntaxin1A available for SNARE interactions.

(Resubmitted 26 April 2004; accepted after revision 11 June 2004; first published online 24 June 2004)
Corresponding author S. E. Gladycheva: 7804 Medical Sciences II Building, Department of Molecular and Integrative Physiology, The Medical School, University of Michigan, Ann Arbor, MI 48109-0622, USA. Email: segladys@umich.edu

Neurotransmitter release at chemical synapses is regulated by calcium influx and accomplished via a set of highly regulated interactions between synaptic vesicle and plasma membrane proteins. Essential to this exocytotic process are interactions between the conserved membrane SNARE proteins syntaxin1A, SNAP25 and VAMP/synaptobrevin. Indeed, membrane fusion requires transient assembly of target membrane and vesicle SNARE motifs into functional four-helix core complexes (Sollner, 2003). Critical to formation of the SNARE core complex is a conformational shift in syntaxin1A that initiates and facilitates interaction of SNARE motifs (Carr, 2001; Rizo & Sudhof, 2002).

Syntaxin1A consists of a carboxyl-terminal transmembrane anchor (residues 256–288), a juxta-membrane α-helical H3 domain (residues 186–238) and an N-terminal domain that consists of an anti-parallel three-helix bundle termed the H_{ABC} domain. The H3 domain contains the SNARE motif (Lerman *et al.* 2000). In addition to SNARE protein interactions, syntaxin1A has been reported to interact with a diverse array of proteins. Of these, voltage-gated calcium channels and Sec1/Munc18 (S/M) family proteins demonstrate direct association with syntaxin1A in mammalian neurones and participate in the exocytotic process (Garcia *et al.* 1994; Catterall, 2000; Yang *et al.* 2000). The interaction of syntaxin1A with N-type and P/Q-type calcium channels results in a negative shift in the steady-state voltage-inactivation relationship, thereby reducing their availability for calcium influx (Bezprozvanny *et al.* 1995; Degtiar *et al.* 2000). This interaction also promotes G-protein inhibitory regulation of channel activation (Stanley & Mirotznik, 1997; Dolphin, 1998; Ikeda & Dunlap, 1999). However, interaction of munc18-1 with syntaxin1A stabilizes syntaxin1A in a conformation where the H_{ABC} domain of syntaxin1A folds and interacts

 DOI: 10.1113/jphysiol.2004.067249

with its H3 domain, thereby hindering interaction of the H3 domain with SNARE proteins (Hanson, 2000; Misura *et al.* 2000). Paradoxically, the association of munc18 with syntaxin1A is also essential for efficient formation of SNARE complexes (Pevsner *et al.* 1994). For example, S/M protein function is essential for vesicle consumption in yeast (Novick & Schekman, 1979; Cowles *et al.* 1994), *Drosophila* (Harrison *et al.* 1994), *C. elegans* (Hosono *et al.* 1992) and for evoked neurotransmitter release at the squid giant synapse (Dresbach *et al.* 1998). Also, munc18-1 deficient mice demonstrate a complete loss of synaptic transmission (Verhage *et al.* 2000). Since munc18 is required for membrane fusion yet stabilizes syntaxin1A in a nonreactive conformation, it necessitates proposal of a mechanism that regulates munc18-1 binding and syntaxin1A activation. Multiple effectors have been proposed, including members of the munc13 (Brose *et al.* 2000), Doc2 (Verhage *et al.* 1997), Rab3 (Webb *et al.* 1997; Tall *et al.* 1999) and tomosyn (Fujita *et al.* 1998) gene families, as well as regulation through catalytic activity of protein kinase C (Barclay *et al.* 2003) and cyclin-dependent kinase 5 (Cdk5) (Shuang *et al.* 1998; Fletcher *et al.* 1999). However, difficulty in reconstituting regulation of the mammalian syntaxin1A–munc18 complex *in vitro* has resulted in considerable uncertainty regarding the physiological importance of these putative regulators. Moreover, the presence of endogenous syntaxin1A, munc18 and multiple SNARE regulatory proteins in neurones, together with multiple VDCC types, has substantially hindered rigorous examination of the regulation of syntaxin1A–channel and syntaxin1A–munc18 interaction within neurones.

The goal of this study was to investigate munc13 regulation of the interaction between munc18 and syntaxin1A in a physiological *in situ* context. We used a functional approach that monitored alterations in the gating properties of N-type voltage-dependent calcium channels (N-VDCC) exogenously expressed in HEK293 cells. The strong influence of syntaxin1A on channel gating provided a sensitive method to assess the capacity of munc18-1 and munc13-1 to influence syntaxin1A protein–protein interactions. Furthermore, to establish whether munc13-1 promoted syntaxin1A activation and competence to form SNARE protein interactions, we evaluated the ability of syntaxin1A to form interactions with a mutant of SNAP25. Our results suggest that munc13-1 is a specific regulator of the syntaxin1A–munc18 interaction and that it promotes activation of syntaxin1A for SNARE complex formation.

Methods

Gene constructs and antibodies

Human embryonic kidney (HEK293) cells stably expressing the rat α_{1B} and human β_{1B} and $\alpha_2\delta$ calcium channel subunits (termed HEK293-S3 cells) were a gift from D. Rock (Warner-Lambert Parke Davis, Ann Arbor, MI, USA). Expression vectors pRc/CMV syntaxin1A (rat) and pGEX-kg GST-munc18 (rat) were provided by R. Scheller (Stanford University, Palo Alto, CA, USA) and subsequently transferred alone or with His(6X)-epitope tag into pcDNA3.1. The LoxP sequence from pLP-EGFP-C1 (Clontech, Palo Alto, CA, USA) was subcloned into the multiple cloning site regions of pFLAG-CMV2, pcDNA3.1, pECFP-C1 and pEcYFP-C1 (Q39M mutant of pEYFP-C1) to generate recipient vectors for subcloning using the *Cre*-recombinase-mediated Creator System (Clontech). Munc18 and syntaxin1A were merged to the C-terminal of ECFP and EcYFP. Mammalian expression constructs for munc13-1, munc13-2 and munc13-3 were provided by N. Brose (Max-Planck-Institut fur Experimentelle Medizin, Gottingen, Germany), and munc13-1 and munc13-3 were fused to the C-terminal of EGFP. PcDNA3-mSNAP-25b (mouse) was provided by T. F. Martin (University of Wisconsin, Madison, WI, USA), subcloned into pDNR-Dual (Clontech) and subjected to PCR-based, site-directed mutagenesis (QuickChange, Stratagene, La Jolla, CA, USA) to alter cysteine residues at positions 85, 88, 90 and 92 to alanine. This mutant cDNA was then subcloned into pFLAG-CMV2 and pLP-EGFP-C1 to generate the epitope-tagged (FLAG-S25 C/A) and fluorescent (GFP-S25 C/A) fusion protein expression constructs by recombination. The sequence fidelity of all constructs was confirmed by DNA sequencing (University of Michigan DNA Sequencing Core).

Antibodies used were as follows: syntaxin1A (clone HPC-1, Sigma); munc18-1 (clone 31, BD Transduction Laboratory, Goettingen, Germany); Munc13-1 (clone 3H5, Synaptic Systems); panMunc13 (clone 32, BD Transduction Laboratory); α_{1B} calcium channel subunit (Alomone Laboratories, Jerusalem, Israel); pFLAG (clone M2 and polyclonal, Sigma); SNAP25 (clone SMI81, Sternberger Monoclonals, Lutherville, MD, USA); syntaxin4 (Synaptic Systems); and SNAP23 (Synaptic Systems).

Cell culture and transfections

HEK293-S3 cells were continuously grown in T-75 flasks in RPMI 1640 media supplemented with 1% L-glutamine,

10% fetal bovine serum, 1% penicillin–streptomycin, 1.2% geneticin and 0.8% hygromycin at 37°C in 95% O_2–5% CO_2. Cells were discarded after 15 passages and replaced with a fresh low-passage aliquot. For electrophysiology experiments cells were transiently transfected with expression plasmids using a calcium phosphate method (Wilson *et al.* 1995). One hour before transfection, cells were replenished with DMEM media supplemented with 1% L-glutamine, 1% nonessential amino acids and 10% fetal bovine serum. Cotransfection with pEGFP-C1 served as a reporter for transfected cells and as a source of plasmid DNA that was adjusted to maintain a constant plasmid DNA concentration for each treatment. Analysis of protein expression in cotransfected cells by immunocytochemistry demonstrated that approximately 95% of EGFP positive cells express the cotransfected protein. Cells were used for electrophysiology 48–56 h after transfection. In biochemical and optical investigations cells were transfected using Lipofectamine 2000 (Invitrogen) according to the manufacturer's instructions.

Electrophysiological methods

Cells were plated on glass coverslips immediately before patch-clamp recording. Recordings were made using an Axopatch 200A amplifier (Axon Instruments, Foster City, CA, USA) together with an ITC-16 AD–DA interface (Instrutech Corp., Great Neck, NY, USA) under the control of Pulse Control software (Herrington, 1995) integrated into IGOR PRO software version 4.02a (Wavemetrics Inc., Lake Oswego, OR, USA). Patch pipettes were pulled on a Sutter Instruments P-87 microelectrode puller using borosilicate glass (1.5 mm o.d., AM Systems, Carlsborg, WA, USA). Pipettes were coated with elastomer (Sylgard, Dow Corning, Midland, MI, USA) to minimize capacitance, and fire polished to 2–4 MΩ resistance. All recordings were made using the amphotericin B perforated patch-clamp method under voltage clamp at room temperature. As a cation selective ionophore, amphotericin B allowed electrical continuance with the cell interior but precluded diffusion of cytosolic proteins into the pipette. Pipettes were filled with a solution containing (mM): CsOH, 115; CH_4O_3S, 115; $MgCl_2$, 1; CsCl, 13; Hepes, 30; $CaCl_2$, 1; and EGTA, 1 (pH 7.3, adjusted with CsOH), with 0.26 mM of amphotericin B added immediately before recording. The extracellular recording solution consisted of (mM): TEA-Cl, 120; $BaCl_2$, 10; $MgCl_2$, 1; glucose, 10; and Hepes, 10 (pH 7.3, adjusted with Tris Base). Ba^{2+} was used as charge carrier to minimize interference from any Ca^{2+}-induced current inactivation or Ca^{2+}-activated signalling pathways. Whole cell conductance and series resistance were compensated electronically to 70%. Current signals were filtered at 5 kHz and digitized at ≥25 kHz. Calcium currents were leak subtracted (P/4 protocol) before analysis. Control inactivation relationships were measured from nontransfected cells and from cells expressing the transfection reporter EGFP. No significant differences were found in inactivation relationships between the control cell types and their measurements have been grouped.

A three-pulse voltage protocol was used to study properties of voltage-dependent steady-state inactivation (SSI). Two 20 ms test pulses to 0 mV from a −100 mV holding potential were separated by a conditioning pulse. Measurement of the voltage dependence of inactivation used 1 s conditioning pulses ranging from −110–0 mV. Application of each three-pulse protocol was separated by a 20 s period at the holding potential to allow recovery from voltage-dependent inactivation. Voltage-dependent steady-state inactivation data were fitted with a Boltzmann function of the form:

$$I/I_0 = base + (max - base)/(1 + \exp(-(V - V_h)/k)),$$

where I/I_0 is the current normalized to maximum current, *max* and *base* are the maximum and base of the curve, V_h is the mid-point of voltage dependence of inactivation and k is the slope factor. The kinetics (i.e. time dependence) of onset of inactivation were measured using conditioning pulses to −60 mV of duration ranging from 0.01 to 100 s (reflecting primarily 'slow' inactivation; Degtiar *et al.* 2000), placed between 20 ms test pulses to 0 mV from a −100 mV holding potential. Data were fitted with a function of the form:

$$I/I_0 = base + (max - base)/(1 + [\tau/t]^n),$$

where I/I_0 is the current normalized to maximum current, *max* and *base* are the maximum and base of the curve, τ is the time constant of inactivation and n is a coefficient reflecting the slope of the curve. Values for the half-inactivation voltage (V_h) and time constant of inactivation (τ) were exclusively used to compare effects of various treatments and were not used as interpretative of mechanism(s). Curve fits to data were made using an iterative, nonlinear least-squares fitting algorithm provided in IGOR PRO software.

SNARE pairing using mutant SNAP25

To determine SNARE–SNARE pairing, FLAG-S25 C/A or GFP-S25 C/A construct were combined with experimental constructs and transfected into cells using Lipofectamine 2000 (Invitrogen, Carlsbad, CA,

USA). In FLAG-S25 C/A experiments, subcellular distribution of the FLAG-tag was determined 48 h following transfection. Cells were rinsed once with physiological saline (PS) containing (mM): NaCl, 140; KCl, 5; $CaCl_2$, 2.2; $MgCl_2$, 1, glucose, 10; and Hepes, 10 (pH 7.4, adjusted with NaOH), and scraped into ice-cold buffer containing 2% sucrose, 1 mM EDTA and 20 mM Tris (pH 7.4) supplemented with 1 mM dithiothreitol (DTT) and a mixture of protease inhibitors (1 μg μl^{-1} each of PMSF, leupeptin, pepstatin and aprotinin). Cells were then gently lysed by Dounce homogenization and nuclei removed by brief centrifugation (800*g* for 3 min at 4°C). Cytoplasmic and membrane components in the collected supernatants were then separated by centrifugation at 100 000*g* for 30 min at 4°C. Membrane fractions were resuspended in immunoprecipitation (IP) buffer containing (mM): NaCl, 150; Tris (pH 7.4), 50; and EDTA, 2; supplemented with 1% Triton X-100, 0.5 mM DTT and the protease inhibitor mixture. Concentrated IP buffer was added to cytosolic fractions to establish a 0.67% Triton X-100 level. Equal amounts of protein for membrane and cytosolic samples were then subjected to immunoprecipitation by monoclonal α-FLAG (clone M2, Sigma) antibody. Incubation was carried out for 90 min at 4°C with rotation, after which protein G beads were added for another 1 h incubation. The beads were then collected (1000*g* for 2 min at 4°C) and washed twice in immunoprecipitation buffer with a final wash in TNM buffer. Samples were then analysed by SDS-electrophoresis and immunoblotting. Blots were probed with polyclonal α-FLAG antibody (Sigma) and HRP-conjugated anti-rabbit antibody. Immunoreactive signals were developed using ECL detection, visualized using a FluoroMax Imager (Bio-Rad, Hercules, CA, USA) and quantified using Quantity-One software (Bio-Rad).

In experiments using the GFP-S25 C/A construct, cells were plated onto elliptical glass-bottomed chambers in 35 mm culture dishes to facilitate optical imaging. Two days following plating, cells were transfected with plasmids encoding the appropriate recombinant proteins. Following a 24–48 h expression period, the culture chambers were mounted on an Olympus IX-71 microscope and continuously superfused with PS (1 ml min^{-1}) at room temperature. The microscope was equipped with a xenon lamp and monochrometer-based illumination system (TILL-Photonics, Pleasanton, CA, USA). Cells were viewed with a 60× water immersion objective (NA = 1.2), illuminated at 488 ± 15 nm, and fluorescence collected through a 525 ± 25 nm bandpass filter (Chroma Technologies, Brattleboro, VT, USA). Images were acquired (200 ms at 20 s intervals) using a CCD TILL-IMAGO QE camera prior to and during a period (10 min) of digitonin permeabilization in an intracellular-like saline. The intracellular-like saline contained (mM): K-glutamate, 139; $MgCl_2$, 2; $CaCl_2$, 1.8; EGTA, 5; and Pipes, 20 (pH 6.6). The EGTA:Ca^{2+} ratio was calculated to set a free [Ca^{2+}] of 97 nM. Intensity profiles of lines transecting fluorescent cells were measured on images offline using TILL-vision software and further analysed using IGOR PRO software.

Confocal microscopy

Cells transfected with ECFP–munc18, EcYFP–syntaxin1A, both ECFP–munc18 and EcYFP–syntaxin1A, EGFP–munc13-1 or EGFP–munc13-3 were cultured on glass coverslips for 24 h following transfection. Cells were then fixed with 4% paraformaldehyde–PS for 15 min, rinsed with PS, quenched in 50 mM NH_4Cl–PS, rinsed and mounted with 75% glycerol–PS on glass slides. Digital confocal fluorescence images were obtained using a Zeiss LSM 510 META microscope, which allowed complete separation of ECFP and EcYFP fluorescence signals by linear unmixing. Control emission spectra for linear unmixing were obtained from cells expressing each fluorophore alone. The effectiveness of the linear unmixing algorithm was validated using cells that highly over-expressed ECFP alone and EcYFP alone. Following linear unmixing no measurable signal was found in the YFP channel for cells expressing ECFP or in the CFP channel for cells expressing EcYFP, even when contrast settings were boosted to maximum. Images were processed using Photoshop 6.0 software (Adobe systems Inc., Mountain View, CA, USA).

Data analysis and statistics

Data were analysed and statistical analysis performed using IGOR PRO and GraphPad Instat software (GraphPad Software Inc., San Diego, CA, USA). Population data were expressed as means ± S.E.M., and statistical significance was determined using Student's unpaired *t* tests or for multiple comparisons using ANOVA with Dunnett's *post hoc* test on normally distributed data. In the case of non-parametric data, a Mann–Whitney *U* test was performed using the original calculated values. Significant differences were defined by $P < 0.05$ and indicated by an asterisk.

Results

Recombinant protein expression in cells and activation properties of N-VDCC

To investigate regulation of the interaction between syntaxin1A and munc18 we have used HEK293-S3 cells

as a heterologous cell expression system. These cells demonstrated no detectable immunoreactive signal for syntaxin1A, munc18-1, or munc13 (Fig. 1*A*). As a result, they offer an advantageous system in which to examine syntaxin1A–munc18 interactions *in situ*. The paralogue SNARE proteins syntaxin4 and SNAP23 that play a role in constitutive secretion and membrane trafficking in epithelial cells were found to be endogenously present in these cells (Fig. 1*A*). Transfection with expression plasmids encoding syntaxin1A, munc18 and munc13 resulted in expression of corresponding recombinant protein. The monoclonal munc13 antibodies used reacted with munc13-1 and weakly with munc13-2 but failed to react with munc13-3. EGFP fused to the N-terminal of munc13-3 was used to visualize its expression (see Fig. 1*C*). Expression levels of syntaxin1A were unaltered by coexpression of munc18, although munc18 levels were decreased upon coexpression with syntaxin1A

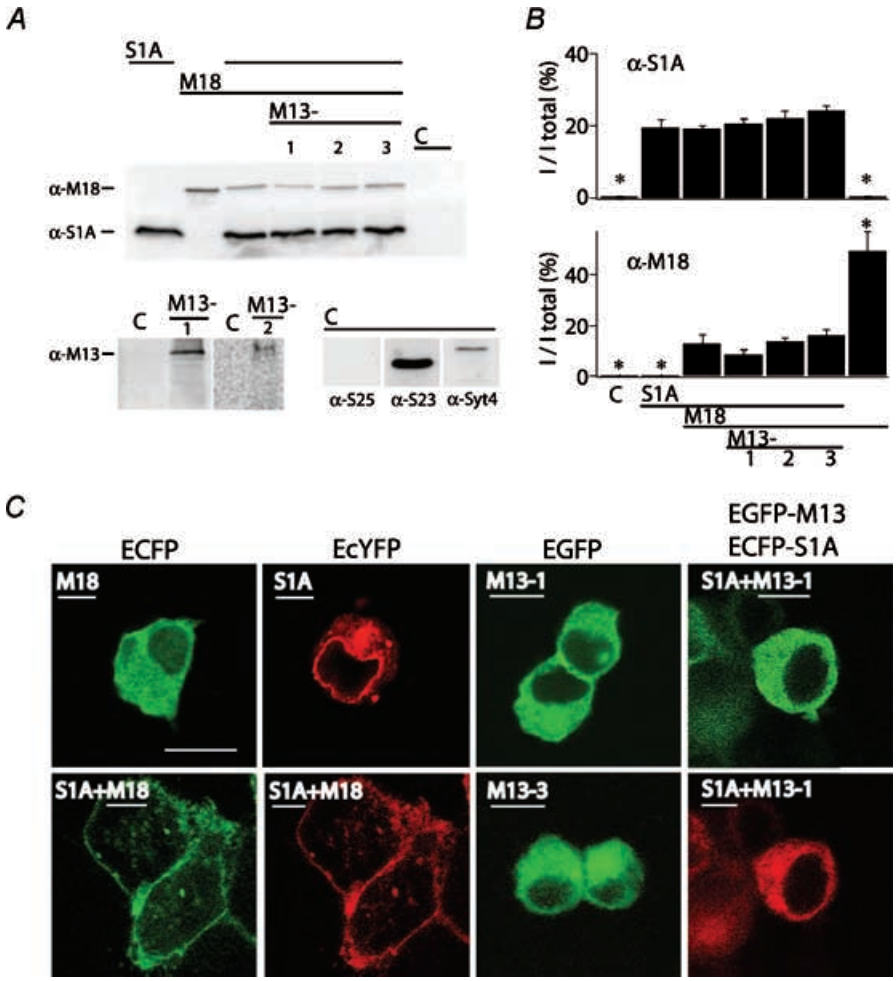

Figure 1. Recombinant protein expression in transfected HEK293-S3 cells
A, upper panel, Western blot showing immunoreactivity against recombinant protein(s) in lysates of control (non-transfected) cells (C) and cells transiently (co)transfected with syntaxin1A (S1A) and munc18 (M18) and munc13 (M13) isoforms: munc13-1 (1), munc13-2 (2) or munc13-3 (3). Lower-left panel, immunoblots showing immunoreactivity against munc13-1 and munc13-3 in cells transiently transfected with corresponding proteins, but not in control cells. Lower-right panel, immunoblots showing absence of SNAP25 (S25) immunoreactive signal, but presence of endogenous SNAP23 (S23) and syntaxin4 (Syt4) immunoreactivity in lysate of control (non-transfected) cells. *B*, average data quantified from immunoblots showing levels of syntaxin1A (upper histogram) and munc18 (lower histogram) expression for each treatment condition. Levels were quantified as intensity relative to total on each blot. $n = 5$ for each treatment. Statistical significance calculated relative to syntaxin1A plus munc18 condition. *C*, confocal images of ECFP, EcYFP or EGFP fluorescence in cells transiently transfected to express proteins as indicated on the panels: ECFP–munc18 alone (M18), EcYFP–syntaxin1A alone (S1A), EGFP–munc13-1 alone (M13-1), EGFP–munc13-3 alone (M13-3). For ECFP–munc18 with EcYFP–syntaxin1A (S1A + M18) and ECFP–syntaxin1A with EGFP–munc13-1 (S1A + M13-1) the images are linearly unmixed with the fluorescent protein underlined.

(Fig. 1*B*). Neither syntaxin1A nor munc18 expression were significantly altered by additional coexpression of munc13 isoforms (Fig. 1*B*).

To examine the subcellular distribution of the recombinant syntaxin1A, munc18 and munc13, EGFP, ECFP or EcYFP fluorescent protein was fused to the N-terminus of each protein. Figure 1*C* shows cells transfected with ECFP–munc18, EcYFP–syntaxin1A, EGFP–munc13-1 or EGFP–munc13-3 alone. ECFP–munc18 fluorescence appeared evenly distributed throughout the cytoplasm, whereas EcYFP–syntaxin1A showed areas of intense fluorescence probably associated with membranous compartments within the cytosol and the perinuclear region. Upon coexpression of ECFP–munc18 with EcYFP–syntaxin1A, a dramatic change in localization of both EcYFP–syntaxin1A and ECFP–munc18 occurred, as reflected by enrichment and general colocalization of fluorescence signals at the plasma membrane (Fig. 1*C*). These data suggest that a functional interaction is established between these proteins upon coexpression. EGFP–munc13-1 and EGFP–munc13-3 were localized to cytosol. The coexpression of EGFP–munc13-1 with ECFP–syntaxin1A did not change the cellular distribution of EGFP–munc13-1.

Overexpression of syntaxin1A in heterologous cell lines that are neurosecretion incompetent can result in alterations in membrane transport of syntaxin1A and eventually in disassembly of the Golgi apparatus (Rowe *et al.* 1999). This possibility prompted us to establish that expression and membrane trafficking of the N-VDCC subunits used for our functional assay remained normal during the period of syntaxin1A expression. Therefore, we compared N-VDCC properties sensitive to β_1 and $\alpha_2\delta$ channel subunit expression, namely, current activation kinetics, current density and the voltage dependence of channel activation. The rate of current activation, measured as the time required to rise from 10 to 90% of the maximal current in response to a step depolarization to 0 mV from a holding potential of −90 mV, was 3.0 ± 1.3 ($n = 17$) and 2.8 ± 0.8 ms ($n = 20$) in the absence and presence of syntaxin1A overexpression, respectively. Representative currents are shown in Fig. 2*A*. Current density distributions also showed similarity between control (EGFP-transfected) and syntaxin1A-transfected cells (Fig. 2*B*). The voltage dependence of current activation (chord conductance–voltage relationships) and corresponding *I–V* relationships are shown in Fig. 2*C* and *D*. A Boltzmann fit of the conductance–voltage curves resulted in a half-activation voltage of -19.9 ± 2.2 ($n = 9$) and -21.4 ± 0.6 mV ($n = 8$) for control and syntaxin1A expressing cells, respectively. Additionally, mean *I–V* relationships for control and syntaxin-expressing cells showed similar shape along the voltage axis. The Ca^{2+} channel blocker Cd^{2+} (100 μM) added to the extracellular medium eliminated the current, confirming Ca^{2+} dependence of the current. The level of expression

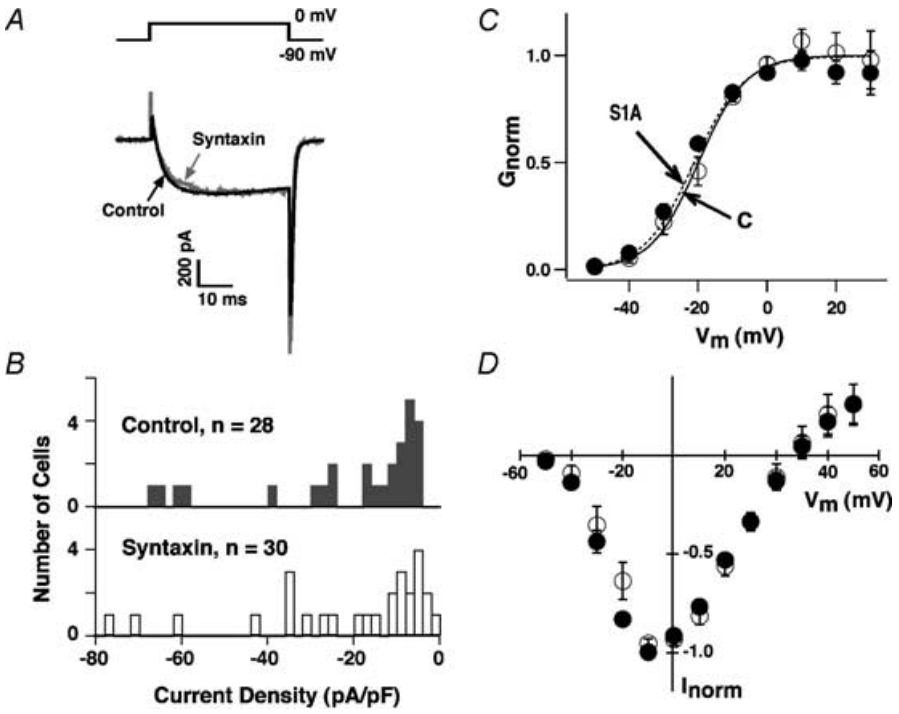

Figure 2. Effects of syntaxin1A on kinetic and voltage-dependent properties of N-VDCC
A, inward Ba^{2+} current evoked in response to a voltage step to 0 mV from a holding potential of −90 mV for syntaxin1A-transfected (grey) and control transfected (pEGFP-C1 parental plasmid; black) cells. *B,* current density histograms determined from control cells and those expressing recombinant syntaxin1A. *C,* conductance–voltage relationship of N-VDCC current activation of control cells (○) and of cells expressing recombinant syntaxin1A (●). N-VDCC conductance at the given voltages was calculated as chord conductance using the reversal potentials from corresponding *I–V* data (*D*). Lines are Boltzmann fits to data.

of syntaxin1A therefore appeared not to substantially alter the trafficking or voltage activation properties of the N-VDCC.

Effects of syntaxin1A and munc18 on voltage-dependent inactivation of N-VDCC

To use N-VDCC inactivation as a reporter of regulation of a syntaxin1A–munc18 complex required establishment of a baseline dataset. Initially, the effect of syntaxin1A expression on channel inactivation in the presence and absence of munc18 was quantified. Inactivation relationships were determined using a three-pulse protocol and measurement of the ratio of current amplitude (I/I_0), where I_0 is the peak current response to an initial test pulse and I is the peak current response to the same test pulse following a conditioning pulse (Fig. 3*A*). To measure the voltage dependence of steady-state inactivation (SSI) a prolonged (1 s) conditioning pulse was applied over a series of conditioning voltages. To examine kinetic effects on the development of inactivation, the effect of duration of the conditioning voltage (extending from 0.01 to 100 s at −60 mV) was determined. The voltage-dependent inactivation relationships show that the −100 mV holding potential and recovery time were sufficient to fully remove inactivation of the N-VDCC between trials. Expression of syntaxin1A shifted the half-inactivation potential to more hyperpolarized potentials ($V_h = -51.1 \pm 0.9$ mV, control; $V_h = -61.1 \pm 1.2$ mV, syntaxin1A) and decreased the time constant of inactivation ($\tau = 2.8 \pm 0.6$ s,

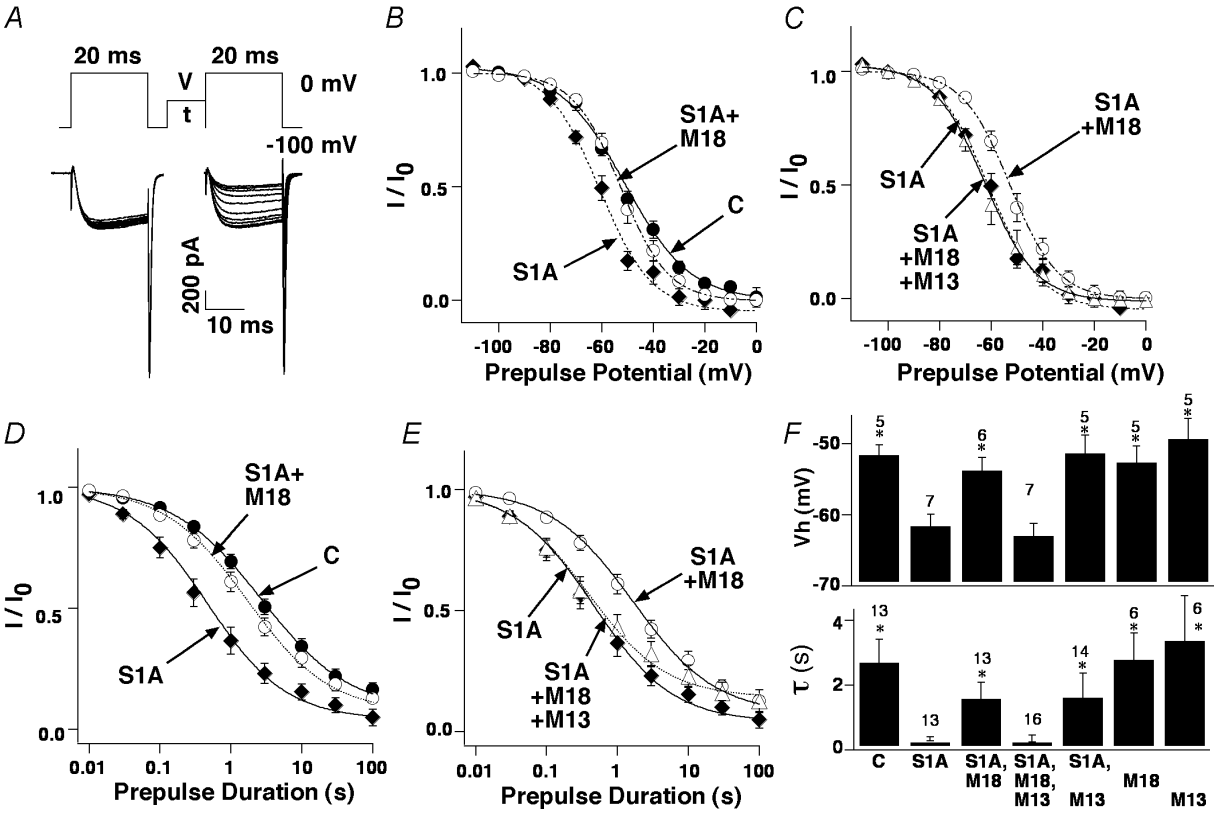

Figure 3. Effects of syntaxin1A, munc18 and munc13-1 expression on inactivation properties of N-VDCC
A, pulse protocol used to determine SSI or time dependence of inactivation of N-VDCC and corresponding representative current responses. *B* and *D,* syntaxin1A (♦) expression enhances sensitivity to SSI (*B*) and accelerates development of inactivation (*D*) from that of control cells (●), while the added expression of munc18 (○) relieves the enhancing effect of syntaxin1A. Normalized current (I/I_0) for each condition is plotted against the 1 s conditioning prepulse potential (*B*) or against the duration, *t*, of the −60 mV conditioning prepulse (*D*). *C* and *E,* munc13-1 expression with syntaxin1A and munc18 (Δ) results in SSI and time course of inactivation relationships left-shifted from those in coexpression of syntaxin1A with munc18 (○). Inactivation relationships for syntaxin1A (♦) are shown for comparison. *F,* average potential of half-inactivation of SSI (V_h, upper histogram) and averaged time constant of inactivation (τ, lower histogram). Values were determined from fits of I/I_0 curves, as described in the Methods. Numbers above bars indicate number of observations. Significant differences are relative to syntaxin1A transfection conditions.

control; $\tau = 0.4 \pm 0.1$ s, syntaxin1A) from control values (Fig. 3*B* and *D*). Importantly, coexpression of munc18 with syntaxin1A resulted in inactivation relationships ($V_h = -53.2 \pm 1.3$ mV and $\tau = 1.7 \pm 0.6$ s) that were significantly different from syntaxin1A treatment. Expression of munc18 in the absence of syntaxin1A had no effect on inactivation ($V_h = -52.1 \pm 1.7$ mV and $\tau = 2.9 \pm 0.7$ s). Average current density values were not significantly different between treatments (30 ± 6 pA pF^{-1}, syntaxin1A; 33 ± 12 pA pF^{-1}, munc18; 29 ± 4 pA pF^{-1}, munc18 with syntaxin1A) and neither were syntaxin1A expression levels (Fig. 1*B*). Relief of the effect of syntaxin1A on the voltage dependence and time course of SSI by munc18 confirms that a functional interaction between syntaxin1A and munc18 occurred in the HEK293-S3 cells.

Effects of munc13 coexpression on inactivation of N-VDCC

Multiple reports have suggested that munc13-1 plays an essential role in the syntaxin1A conformational cycle (Betz *et al.* 1997; Sassa *et al.* 1999; Richmond *et al.* 2001). To test the possibility that munc13 regulates the syntaxin1A–munc18 complex, we measured the effect of munc13-1 coexpression with syntaxin1A and munc18 on the N-VDCC inactivation relationships. Using this multiple expression condition, we observed the voltage- and time-dependent relationships of inactivation ($V_h = -62.4 \pm 2.0$ mV and $\tau = 0.4 \pm 0.1$ s) to be left-shifted from those of syntaxin1A with munc18 expression, but not significantly different from those found with expression of syntaxin1A alone (Fig. 3*C* and *E*). Average current density values remained consistent with those of prior treatments (28 ± 8 pA pF^{-1}). The average half-inactivation potentials and time constants of inactivation for each treatment are shown in Fig. 3*F*. Taken together, these data are consistent with the hypothesis that munc13-1 alters the munc18–syntaxin1A complex and mediates changes in syntaxin1A protein–protein interactions.

Munc13-1 is a phorbol ester and diacylglycerol binding protein that demonstrates a variety of protein interactions and is enriched in the cytomatrix of the presynaptic active zone (Martin, 2002). This multifunctional nature of munc13-1 raised the possibility that its effects on N-VDCC inactivation may occur independently of munc18–syntaxin1A complex regulation. For example, munc13 may compete with munc18 for syntaxin1A binding, or may activate a signalling pathway independent from syntaxin1A that leads to regulation of N-VDCC gating. To determine if the effects of munc13-1 on inactivation required interaction with the syntaxin1A–munc18 complex, we tested the effects of expression of munc13-1 with syntaxin1A, and munc13-1 alone. The average results of these treatments are shown in Fig. 3*F*. For coexpression of munc13-1 with syntaxin1A, the half-inactivation potential and time constant of inactivation ($V_h = -50.8 \pm 2.0$ mV and $\tau = 1.7 \pm 0.6$ s) were similar to those observed for expression of syntaxin1A with munc18. Moreover, munc13-1 expression in the absence of syntaxin1A also resulted in average inactivation parameters of $V_h = -48.8 \pm 2.3$ mV and $\tau = 3.5 \pm 1.3$ s. Therefore, syntaxin1A and munc18, syntaxin1A and munc13, and munc13-only treatments resulted in identical inactivation properties. Since these properties were distinct from those of the syntaxin1A plus munc18 plus munc13 treatment, it is unlikely that the inactivation phenotype observed in syntaxin1A plus munc18 plus munc13 treatment resulted from simple competitive binding between munc18 and munc13 for syntaxin1A. Taken together, the ability of munc13-1 to reduce τ and enhance voltage sensitivity of SSI in the presence of munc18 and syntaxin1A is consistent with the hypothesis that munc13-1 interacts with a munc18–syntaxin1A complex to promote a change in syntaxin1A interactions.

Munc13 has three different isoforms: munc13-1, munc13-2 (including brain-specific b-munc13-2 and ubiquitous ub-munc13-2) and munc13-3. The three isoforms share a common, highly homologous C-terminal domain that has been demonstrated to be important for direct syntaxin1A interaction, but differ in their N-terminal domains (Brose *et al.* 2000). To determine whether the observed regulation of the syntaxin1A–munc18 complex by munc13-1 is isoform specific, we tested the effects of munc13-2 and munc13-3 expression. As shown in Fig. 4*A* and *B*, expression of munc13-2 or munc13-3 together with syntaxin1A demonstrated half-inactivation potentials ($V_h = -54.6 \pm 1.0$ mV for munc13-2 and -55.3 ± 2.0 mV for munc13-3) and time constants ($\tau = 2.2 \pm 0.7$ s for munc13-2 and 2.3 ± 1.0 s for munc13-3) similar to those of munc13-1 with syntaxin1A. Expression of munc13-2 or munc13-3 with syntaxin1A and munc18 together resulted in inactivation properties ($V_h = -47.5 \pm 1.6$ mV, $\tau = 1.9 \pm 0.3$ s for munc13-2 and $V_h = -48.0 \pm 1.7$ mV, $\tau = 1.6 \pm 0.3$ s for munc13-3) similar to those in treatments without munc18 (Fig. 4*C* and *D*). Average values for half-inactivation potentials and for time constants for all these treatments are compared in Fig. 4*E* and *F*. Thus, although munc13-2 and munc13-3 are capable of interacting with syntaxin1A and altering

its effect on the inactivation properties of N-VDCC, neither munc13-2 nor munc13-3 replicated the effect of munc13-1 in coexpression with syntaxin1A and munc18. Therefore, regulation of the syntaxin1A–munc18 complex by munc13 appears to be munc13-1 isoform specific.

Effects of munc13 on syntaxin1A–SNARE interactions

The above electrophysiological data demonstrated specific syntaxin1A protein–protein interactions that may alter syntaxin1A interaction with N-VDCC. To elucidate whether these protein–protein interactions promoted competency of syntaxin1A for SNARE core complex formation we tested whether these interactions promoted interaction of syntaxin1A with its cognate t-SNARE, SNAP25. The experiments used a SNAP25 mutant that contained an N-terminal epitope FLAG tag in which the four normally palmitoylated cysteine residues of SNAP25 that direct membrane targeting were mutated to alanine (termed FLAG-S25 C/A). In this manner the cytosol-localized FLAG-S25 C/A would become membrane localized only when the H3 domain of syntaxin1A was available for pairing. The subcellular distribution of FLAG-S25 C/A was determined by subcellular fractionation via ultracentrifugation of detergent-free cell lysates to separate cytosol and membrane-delimited fractions. Figure 5 shows that expression of FLAG-S25 C/A alone resulted in little FLAG-S25 C/A being membrane localized while its coexpression with syntaxin1A substantially increased membrane-associated FLAG-S25 C/A. Munc13-1 and syntaxin1A coexpression also resulted in membrane localization of FLAG-S25 C/A. However, the combined expression of

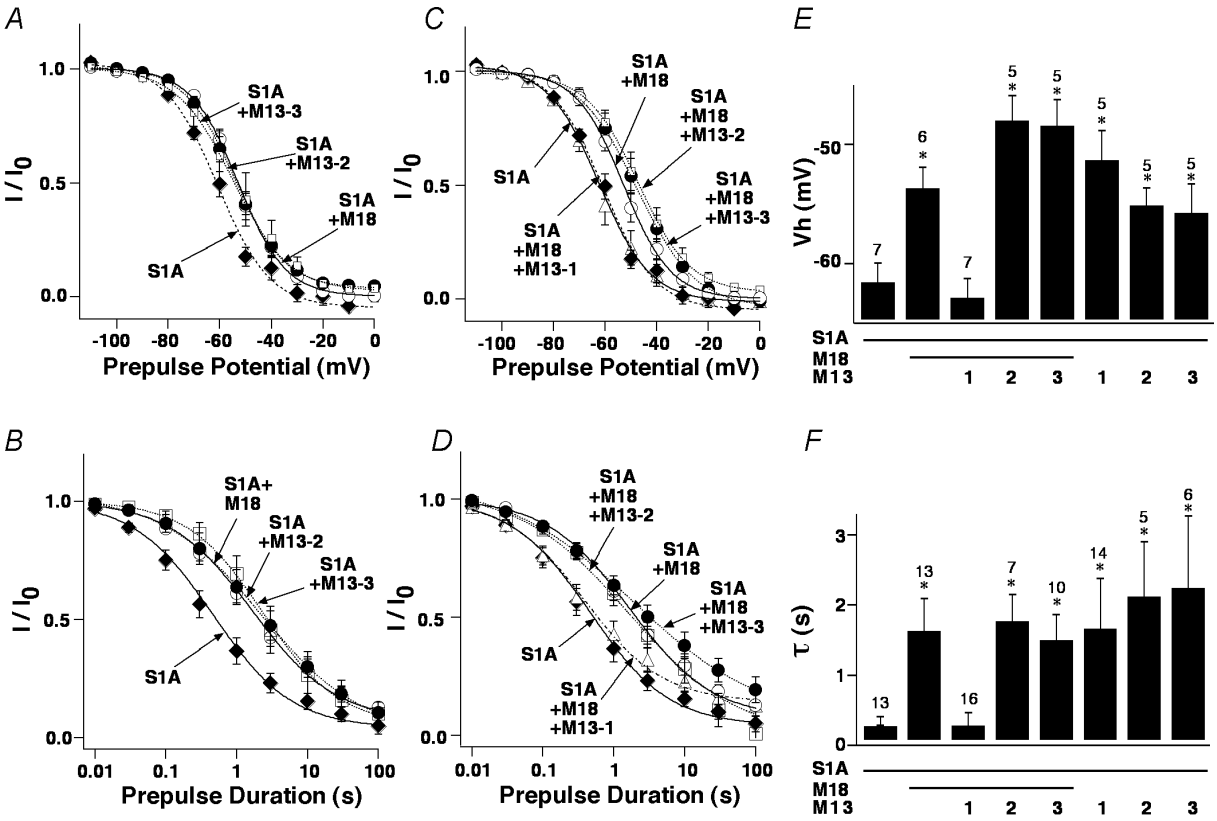

Figure 4. Effects of munc13-2 and munc13-3 isoforms on the time course of inactivation of N-VDCC
A and *B*, syntaxin1A plus munc13–2 (□) and syntaxin1A + munc13–3 (●) effect on voltage dependence and time dependence of inactivation. Inactivation relationships for syntaxin1A (♦) and syntaxin1A plus munc18 (○) are shown for comparison. *C* and *D*, effects of coexpression of munc13 isoforms (munc13-1, Δ; munc13-2, □; and munc13-3, ●) with syntaxin1A and munc18 on voltage dependence and time dependence of channel inactivation. Normalized current (I/I_0) for each condition is plotted against the 1 s conditioning prepulse potential (*A* and *B*) or against the duration, *t*, of the −60 mV conditioning prepulse (*C* and *D*). *E*, average half-inactivation potential determined from I/I_0 relationships. *F*, average time constant of inactivation (τ) determined from I/I_0 relationships. Significant differences are relative to the syntaxin1A treatment.

FLAG-S25 C/A with syntaxin1A and munc18 reversed the membrane localizing effect of syntaxin1A. Most importantly, reduction in the FLAG-S25 C/A signal resulting from munc18 coexpression with syntaxin1A was significantly reversed on the added expression of munc13.

To complement these experiments we used an N-terminal GFP-tagged S25 C/A construct to allow optical visualization of changes in S25 C/A distribution in live cells that had been transfected and expressed different combinations of syntaxin1A and interacting proteins. To reduce the cytosolic GFP-S25 C/A signal and isolate the contribution of the membrane-delimited fluorescence signal, images of the fluorescence signal were taken before and after membrane permeabilization with digitonin. As shown in Fig. 6*A*, GFP-S25 C/A was largely cytosolic when expressed alone or in combination with syntaxin1A plus munc18, as indicated by loss of fluorescence signal upon permeabilization (representative of the unbound GFP-S25 C/A diffusion into the bulk solution). In comparison, coexpression of GFP-S25 C/A with syntaxin1A or GFP-S25 C/A with syntaxin1A, munc18 and munc13-1 leads to a distribution of the fluorescence signal that is membrane delimited and is retained following permeabilization of the plasma membrane with digitonin. Average values among the treatments are presented in Fig. 6*B*. Munc13-1 expression with syntaxin1A also resulted in the membrane-delimited GFP-S25 C/A signal, although reduced in magnitude from that observed with munc13-1 plus munc18 plus syntaxin1A expression. Expression of munc13-1 alone did not recruit GFP-S25 C/A to the membrane. The results from the biochemical subcellular fractionation and the visualization of distribution changes using GFP-S25 C/A are largely consistent. They demonstrate that syntaxin1A can interact with S25 C/A to localize it to the membrane, that munc18 stabilizes syntaxin1A in a state whereby an interaction with S25 C/A is inhibited, and that munc13-1 acts to promote syntaxin1A interaction with S25 C/A in the presence of munc18 coexpression. The only substantial difference between results of the assays occurred in the syntaxin1A plus munc13-1 condition. In this case, the FLAG-S25 C/A showed strong membrane association while GFP-S25 C/A membrane association was more modest. The underlying cause for this difference is not known, although it is possible that this specific protein complex is more sensitive to digitonin permeabilization.

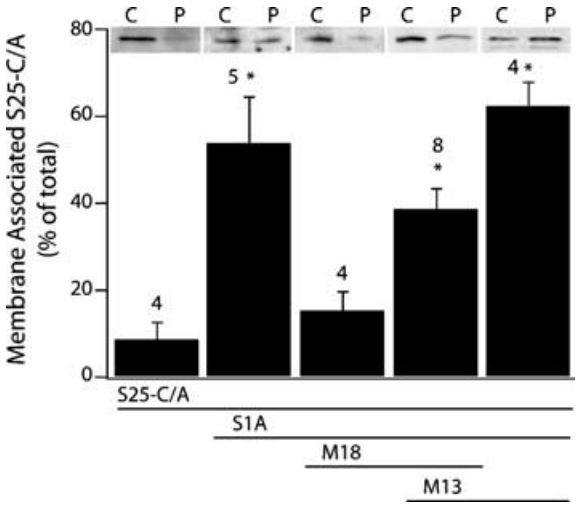

Figure 5. Distribution of FLAG-SNAP25 mutant in cells expressing syntaxin1A and syntaxin1A-interacting proteins
Treatments are indicated below histogram. Values plotted are averaged percentage of FLAG-S25 C/A immunoreactivity found in a particulate fraction ((particulate signal/total signal) × 100). A digital image of the immunoblot ECL signal was taken using a cooled CCD camera (Fluoromax S; Bio-Rad) and the mean intensity of the bands representing immunoreactivity and of adjacent mean background signals was quantified from the digital images using QuantityOne Software (Bio-Rad). Total plasmid DNA for each condition was kept constant across conditions by use of empty parent plasmid. Significant differences are relative to S25 C/A treatment. Representative immunoblots (α-FLAG) corresponding to treatments are shown above histogram (C, cytosolic; P, membranes).

Discussion

In the present study, we used inactivation properties of N-VDCC to understand the regulation of syntaxin1A protein–protein interactions in a mammalian system *in vivo*. We demonstrated that syntaxin1A expression enhanced the voltage sensitivity of steady-state inactivation and accelerated entry of N-VDCC into inactivation. These effects were relieved on coexpression of munc18. Importantly, munc13-1, but not munc13-2 or munc13-3, coexpression reestablished the enhancement by syntaxin1A of N-VDCC inactivation when munc18 was present. Moreover, we demonstrated that munc18 was critical for munc13-1 to exert this regulatory action. This suggests that competition between munc13 and munc18 for syntaxin1A binding was unlikely to account for the regulation. The specificity of regulation to munc13-1 was not related to a unique ability to alter the functional interaction of syntaxin1A with N-VDCCs, since munc13-2 and munc13-3 were also observed to eliminate an enhancing effect of syntaxin1A on inactivation in the absence of munc18. In addition, we report that the regulatory action of munc13-1 on the syntaxin1A–munc18 complex promoted activation of syntaxin1A for SNARE pairing. For example, a mutant

SNAP25 lacking its membrane targeting sites remained cytosolic on coexpression of syntaxin1A with munc18, but became membrane delimited with the added expression of munc13-1. Taken together, the findings of the present study indicate a specific regulatory action of munc13-1 upon the syntaxin1A–munc18 complex in mammalian cells that facilitates activation of syntaxin1A for SNARE core complex formation.

Syntaxin1A protein–protein interactions and N-VDCC inactivation properties

Syntaxin1A has repeatedly been reported to interact with N-type (α_{1B}) voltage-gated Ca^{2+} channels (Rettig *et al.* 1996; Walker & De Waard, 1998; Catterall, 2000). Interaction has been mapped to multiple sites, including the transmembrane domain of syntaxin1A, the H3 SNARE motif, and the N-terminal region. Functional consequences of these interactions on N-VDCC include an enhancement in voltage-dependent SSI (Bezprozvanny *et al.* 1995; Wiser *et al.* 1996; Degtiar *et al.* 2000) and an increase in sensitivity to tonic inhibition by G-protein $\beta\gamma$ subunits (Stanley & Mirotznik, 1997; Dolphin, 1998; Jarvis *et al.* 2000; Lu *et al.* 2001). Our data showed that coexpression of munc18 with syntaxin1A removed the enhancing effects of syntaxin1A on inactivation of N-VDCC. These observations are in agreement with those of (Jarvis & Zamponi, 2001). The crystal structure of syntaxin–munc18 in complex has demonstrated that this bimolecular interaction stabilizes a folded conformation of syntaxin1A that makes the H3 SNARE motif unable to participate in SNARE complex formation (Dulubova *et al.* 1999; Misura *et al.* 2000) and, consistent with our data, in interactions with N-VDCC.

An important finding of our experiments was that the syntaxin1A–munc18 interaction could be specifically affected by munc13-1 coexpression. This conclusion was based in part on results showing that the combined expression of munc13-1, munc18 and syntaxin1A resulted in channel inactivation characteristics distinctly different from those observed in syntaxin1A–munc18 or syntaxin1A–munc13 treatments. Moreover, munc18 or munc13-1 expression alone failed to alter voltage or time dependence of N-VDCC inactivation. Certainly, there is considerable biochemical and genetic evidence to support munc13 as a regulator of the transition of syntaxin1A from its munc18-bound to an activated state ready for SNARE–SNARE interaction. For example, a conserved domain of 165 amino acids between second and third C2 domains of the C-terminal half of munc13-1 exhibits a direct

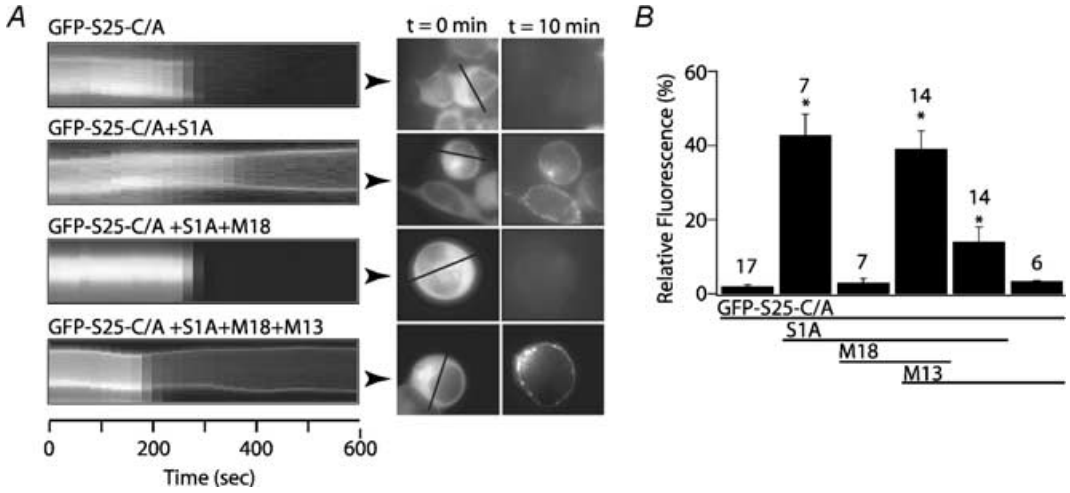

Figure 6. Use of EGFP-S25 C/A mutant as an optical reporter for munc13-1-mediated syntaxin1A–SNARE pairing

A, images (right) and line-intensity profile plots (left) of cells cotransfected with the given combination of proteins. Images were captured before, and during a 10 min period of digitonin treatment (20 μM). Lines transecting representative cells for each treatment (black lines) were used to generate intensity profiles that were collated (20 s bins) to generate stacked line-intensity plots. Digitonin permeabilization begins at $t = 60$ s. Note that for GFP-S25 C/A plus S1A and GFP-S25 C/A plus S1A plus M18 plus M13 a fluorescence signal is retained at the cell membrane throughout digitonin treatment. The intensity of cell images (right) at $t = 10$ min was set at 2 × the intensity of $t = 0$ to enhance visualization. *B*, average data showing cellular EGFP fluorescence remaining in each condition after 10 min of digitonin permeabilization relative to initial fluorescent signal. Numbers above bars indicate number of observations. Significant differences are relative to S25 C/A.

interaction with N-terminal H_{ABC} domain of syntaxin1A (Betz *et al.* 1997; Brose *et al.* 2000). Also, munc13-1 and its *C. elegans* homologue unc13-1 are absolutely essential for vesicle priming, a process that, in part, is believed to involve formation of SNARE core complexes (Brose *et al.* 2000; Martin, 2002). The necessity of munc18 for munc13-1 to enhance voltage-dependent inactivation in our study is consistent with a reported direct interaction between an N-terminal domain (residues 1–266) of *C. elegans* unc13 and unc18 *in vitro* (Sassa *et al.* 1999). Interaction between this homologous pair resulted in release of *C. elegans* syntaxin, Ce64, that lacked its transmembrane domain, from a preformed unc18–Ce64 complex. In mammalian systems, however, a direct interaction between munc18 and munc13 has not been observed (Betz *et al.* 1997). Additional evidence indicating a role of munc13 in activation of syntaxin was provided in experiments which established that a constitutively open syntaxin mutant in *C. elegans* could bypass the requirement for munc13 in vesicle priming (Richmond *et al.* 2001). To date, experimental results confirming that munc13 acts directly upon the syntaxin1A–munc18 complex to faciltate SNARE core complex formation have been missing in mammalian systems.

Since munc13-1 coexpression with syntaxin1A and munc18 resulted in enhanced sensitivity of N-VDCC to inactivation, it is likely that syntaxin1A was released from stabilization by munc18 and interacted with the N-VDCC. An absence of cognate SNAREs for pairing to the newly activated syntaxin1A in this non-neuronal cell line probably promoted its association with N-VDCC. Since munc13-1 plus syntaxin1A and munc18 plus syntaxin1A exerted similar effects on inactivation, the distinct effect observed in the syntaxin1A plus munc18 plus munc13-1 treatment probably did not result from competition between munc18 and munc13-1 for syntaxin1A, but rather, munc13-1 directly dissociated the syntaxin1A–munc18 complex. This dissociation is probably an important reaction for priming in membrane fusion reactions. For example, gene knockout studies in *C. elegans*, *Drosophila* and mice showed that unc13/dunc13/munc13 deletion mutations dramatically reduced both spontaneous and evoked neurotransmitter release without affecting the levels of docked vesicles (Aravamudan *et al.* 1999; Augustin *et al.* 1999*b*; Richmond *et al.* 1999). Also, overexpression of munc13 in chromaffin cells leads to a dramatic increase in a number of release-competent vesicles (Ashery *et al.* 2000). Furthermore, diacylglycerol binding by munc13 has been shown to control presynaptic short-term plasticity and regulate the readily releasable pool of synaptic vesicles (Rhee *et al.* 2002; Rosenmund *et al.* 2002).

Since munc13-1 is a member of a gene family that consists of at least three different munc13 genes, it was important to determine whether the ability to regulate the syntaxin1A–munc18 complex extended to other munc13 isoforms. Munc13-1 and munc13-3 are neural and endocrine cell specific, while munc13-2 has brain-specific (b-munc13-2) and ubiquitous (ub-munc13-2) splice variants (Song *et al.* 1998; Augustin *et al.* 1999*a*). Munc13-3 and b-munc13-2 differ in N-terminal structure from munc13-1, in part, by a deficiency of an N-terminal C2 domain (Brose *et al.* 2000). We found that munc13-3 and b-munc13-2 coexpression with syntaxin1A altered the effect of syntaxin1A on channel inactivation in the same manner as munc13-1, thereby establishing their interaction with syntaxin1A. In contrast, neither munc13-3 nor munc13-2 exerted regulatory activity on syntaxin1A in the presence of munc18, which demonstrated munc13-1 as the isoform critical to regulation. Although the binding site for syntaxin1A is within the C-terminal half of munc13, a lack of regulatory effect by b-munc13-2 and munc13-3 suggests that the N-terminal region of munc13 may be integral for specificity or mechanism of action (Betz *et al.* 1997). These findings are consistent with reports on munc13-1 knockout mice that demonstrated severe consequences for neurotransmitter release in glutamatergic neurones, whereas munc13-2 and munc13-3 knockout mice showed only mild deviation from control animals (Varoqueaux *et al.* 2002). Correspondingly, hippocampal synapses show differences in short-term plasticity characteristics attributable to munc13-1 and munc13-2 (Rosenmund *et al.* 2002).

Implications of munc13-1 action on syntaxin1A SNARE–SNARE pairing

An important goal of our study was to establish conditions that result in activation of syntaxin1A for competency to form SNARE core complexes. Here we used alteration in the distribution of a cytosolic S25 C/A mutant (Vogel *et al.* 2000; Washbourne *et al.* 2001) to assess syntaxin1A availability for SNARE pairing. This mutant retains the ability to form into a SNARE complex and, in addition, reduces SNARE complex disassembly by α-SNAP and N-ethylmaleimide-Sensitive factor (NSF). We found that, while S25 C/A expression alone resulted in little S25 C/A being membrane localized, its coexpression with syntaxin1A or syntaxin1A plus munc13-1 substantially increased its membrane association. Coexpression of munc18 with syntaxin1A in

the presence of S25 C/A reversed the membrane-localizing effect of syntaxin1A on S25 C/A. Most importantly, this effect of munc18 on S25 C/A distribution was relieved with the additional expression of munc13-1. These data are consistent with the following molecular model. Syntaxin1A expressed by itself flickers between SNARE-interacting and noninteracting states (Dulubova *et al.* 2001), which correspond to its channel-interacting and noninteracting states. When no cognate SNARE is present and munc18 is not expressed, channel interaction predominates and a resulting negative shift in SSI occurs. Munc18 binding to syntaxin1A would hold syntaxin1A in a folded inactive conformation for SNARE-pairing or channel regulation. In this situation, the addition of munc13 would promote binding of munc13 to the N-terminus of syntaxin1A, causing munc18 to dissociate, thereby facilitating a change in syntaxin1A conformation to reveal its SNARE motif. In the presence of a cognate SNARE, this reaction would result in SNARE–SNARE pairing and loss of calcium channel regulation by syntaxin1A. Munc13 binding would then transiently remain, consistent with a report demonstrating that a subpopulation of munc13 that interacts with syntaxin1A also interacts with SNAP25/VAMP (Betz *et al.* 1997). In the absence of a cognate SNARE, both munc18 and munc13 would be released, resulting in reestablishment of syntaxin1A interaction with the channel and induction of a negative shift in SSI. When only syntaxin1A and munc13-1 are expressed, the interaction of munc13-1 with the N-terminus of syntaxin1A would be more stable than in the presence of munc18. This would ameliorate the effects of syntaxin1A on the channel SSI. While the above model is consistent with our observations, alternative possibilities exist. For example, promoting effects of syntaxin1A on SSI with combined expression of syntaxin1A, munc18 and munc13 could result from munc18 causing dissociation of preassembled syntaxin1A–munc13 complexes, although this is counter to reports suggesting that munc13 functions downstream of munc18 (Augustin *et al.* 1999*b*; Ashery *et al.* 2000; Weimer *et al.* 2003). Moreover, our results do not rule out the possibility that munc13 and munc18 form complexes, which prevent either from interacting with syntaxin1A. However, unlike for *C. elegans unc*18 and *unc*13, direct interactions between munc18 and munc13 have not been found (Betz *et al.* 1997).

It has been frequently proposed that the N-VDCC–syntaxin1A interaction is of functional importance both in localizing the secretory machine to sites of calcium influx and in coordinating the activation state of the channel to the state of the SNARE core complex. This hypothesis is based on results from *Aplysia* neurones (Smirnova *et al.* 1995) and mammalian nerve terminals (Bergsman & Tsien, 2000), which demonstrated that syntaxin attenuates calcium channel activity. Our results suggest that the functional interaction of syntaxin1A with the channel has a dynamic nature, probably changing according to the state of the SNAREs and formation of the SNARE core complex. Moreover, here we show that munc13-1 is probably critical to regulation of syntaxin1A protein–protein interactions and in mediating activation of syntaxin1A for SNARE–SNARE interactions necessary for membrane fusion. Future investigations are required to confirm munc13 regulation, particularly using methods that report direct protein interactions, and to determine the relevance of this pathway in a neuronal cell preparation.

References

Aravamudan B, Fergestad T, Davis WS, Rodesch CK & Broadie K (1999). Drosophila UNC-13 is essential for synaptic transmission. *Nature Neuroscience* **2**, 965–971.

Ashery U, Varoqueaux F, Voets T, Betz A, Thakur P, Koch H, Neher E, Brose N & Rettig J (2000). Munc13-1 acts as a priming factor for large dense-core vesicles in bovine chromaffin cells. *EMBO J* **19**, 3586–3596.

Augustin I, Betz A, Herrmann C, Jo T & Brose N (1999*a*). Differential expression of two novel Munc13 proteins in rat brain. *Biochem J* **337**, 363–371.

Augustin I, Rosenmund C, Sudhof TC & Brose N (1999*b*). Munc13-1 is essential for fusion competence of glutamatergic synaptic vesicles. *Nature* **400**, 457–461.

Barclay JW, Craig TJ, Fisher RJ, Ciufo LF, Evans GJ, Morgan A & Burgoyne RD (2003). Phosphorylation of Munc18 by protein kinase C regulates the kinetics of exocytosis. *J Biol Chem* **278**, 10538–10545.

Bergsman JB & Tsien RW (2000). Syntaxin modulation of calcium channels in cortical synaptosomes as revealed by botulinum toxin C1. *J Neuroscience* **20**, 4368–4378.

Betz A, Okamoto M, Benseler F & Brose N (1997). Direct interaction of the rat unc-13 homologue Munc13-1 with the N terminus of syntaxin. *J Biol Chem* **272**, 2520–2526.

Bezprozvanny I, Scheller RH & Tsien RW (1995). Functional impact of syntaxin on gating of N-type and Q-type calcium channels. *Nature* **378**, 623–626.

Brose N, Rosenmund C & Rettig J (2000). Regulation of transmitter release by Unc-13 and its homologues. *Current Opinion Neurobiol* **10**, 303–311.

Carr CM (2001). The taming of the SNARE. *Nature Structural Biol* **8**, 186–188.

Catterall WA (2000). Structure and regulation of voltage-gated Ca^{2+} channels. *Annu Rev Cell Dev Biol* **16**, 521–555.

Cowles CR, Emr SD & Horazdovsky BF (1994). Mutations in the VPS45 gene, a SEC1 homologue, result in vacuolar protein sorting defects and accumulation of membrane vesicles. *J Cell Sci* **107**, 3449–3459.

Degtiar VE, Scheller RH & Tsien RW (2000). Syntaxin modulation of slow inactivation of N-type calcium channels. *J Neuroscience* **20**, 4355–4367.

Dolphin AC (1998). Mechanisms of modulation of voltage-dependent calcium channels by G proteins. *J Physiol* **506**, 3–11.

Dresbach T, Burns ME, O'Connor V, DeBello WM, Betz H & Augustine GJ (1998). A neuronal Sec1 homolog regulates neurotransmitter release at the squid giant synapse. *J Neuroscience* **18**, 2923–2932.

Dulubova I, Sugita S, Hill S, Hosaka M, Fernandez I, Sudhof TC & Rizo J (1999). A conformational switch in syntaxin during exocytosis: role of munc18. *EMBO J* **18**, 4372–4382.

Dulubova I, Yamaguchi T, Wang Y, Sudhof TC & Rizo J (2001). Vam3p structure reveals conserved and divergent properties of syntaxins. *Nature Structural Biol* **8**, 258–264.

Fletcher AI, Shuang R, Giovannucci DR, Zhang L, Bittner MA & Stuenkel EL (1999). Regulation of exocytosis by cyclin-dependent kinase 5 via phosphorylation of Munc18. *J Biol Chem* **274**, 4027–4035.

Fujita Y, Shirataki H, Sakisaka T, Asakura T, Ohya T, Kotani H, Yokoyama S, Nishioka H, Matsuura Y, Mizoguchi A, Scheller RH & Takai Y (1998). Tomosyn: a syntaxin-1-binding protein that forms a novel complex in the neurotransmitter release process. *Neuron* **20**, 905–915.

Garcia EP, Gatti E, Butler M, Burton J & De Camilli P (1994). A rat brain Sec1 homologue related to Rop and UNC18 interacts with syntaxin. *Proc Natl Acad Sci U S A* **91**, 2003–2007.

Hanson PI (2000). Sec1 gets a grip on syntaxin. *Nature Structural Biol* **7**, 347–349.

Harrison SD, Broadie K, van de Goor J & Rubin GM (1994). Mutations in the *Drosophila* Rop gene suggest a function in general secretion and synaptic transmission. *Neuron* **13**, 555–566.

Herrington J, Newton K & Bookman R (1995). Pulse control V4.5: IGOR XOPs for patch clamp data acquistion and capaticance measurements. University of Miami, Miami, FL, USA..

Hosono R, Hekimi S, Kamiya Y, Sassa T, Murakami S, Nishiwaki K, Miwa J, Taketo A & Kodaira KI (1992). The unc-18 gene encodes a novel protein affecting the kinetics of acetylcholine metabolism in the nematode *Caenorhabditis elegans*. *J Neurochem* **58**, 1517–1525.

Ikeda SR & Dunlap K (1999). Voltage-dependent modulation of N-type calcium channels: role of G protein subunits. *Adv Second Messenger Phosphoprotein Research* **33**, 131–151.

Jarvis SE, Magga JM, Beedle AM, Braun JE & Zamponi GW (2000). G protein modulation of N-type calcium channels is facilitated by physical interactions between syntaxin 1A and $G\beta\gamma$. *J Biol Chem* **275**, 6388–6394.

Jarvis SE & Zamponi GW (2001). Distinct molecular determinants govern syntaxin 1A-mediated inactivation and G-protein inhibition of N-type calcium channels. *J Neuroscience* **21**, 2939–2948.

Lerman JC, Robblee J, Fairman R & Hughson FM (2000). Structural analysis of the neuronal SNARE protein syntaxin-1A. *Biochemistry* **39**, 8470–8479.

Lu Q, AtKisson MS, Jarvis SE, Feng ZP, Zamponi GW & Dunlap K (2001). Syntaxin 1A supports voltage-dependent inhibition of α_{1B} Ca^{2+} channels by $G\beta\gamma$ in chick sensory neurons. *J Neuroscience* **21**, 2949–2957.

Martin TF (2002). Prime movers of synaptic vesicle exocytosis. *Neuron* **34**, 9–12.

Misura KM, Scheller RH & Weis WI (2000). Three-dimensional structure of the neuronal-Sec1-syntaxin 1a complex. *Nature* **404**, 355–362.

Novick P & Schekman R (1979). Secretion and cell-surface growth are blocked in a temperature-sensitive mutant of *Saccharomyces cerevisiae*. *Proc Natl Acad Sci U S A* **76**, 1858–1862.

Pevsner J, Hsu SC, Braun JE, Calakos N, Ting AE, Bennett MK & Scheller RH (1994). Specificity and regulation of a synaptic vesicle docking complex. *Neuron* **13**, 353–361.

Rettig J, Sheng ZH, Kim DK, Hodson CD, Snutch TP & Catterall WA (1996). Isoform-specific interaction of the α_{1A} subunits of brain Ca^{2+} channels with the presynaptic proteins syntaxin and SNAP-25. *Proc Natl Acad Sci U S A* **93**, 7363–7368.

Rhee JS, Betz A, Pyott S, Reim K, Varoqueaux F, Augustin I, Hesse D, Sudhof TC, Takahashi M, Rosenmund C & Brose N (2002). β phorbol ester- and diacylglycerol-induced augmentation of transmitter release is mediated by Munc13s and not by PKCs. *Cell* **108**, 121–133.

Richmond JE, Davis WS & Jorgensen EM (1999). UNC-13 is required for synaptic vesicle fusion in *C. elegans*. *Nat Neurosci* **2**, 959–964.

Richmond JE, Weimer RM & Jorgensen EM (2001). An open form of syntaxin bypasses the requirement for UNC-13 in vesicle priming. *Nature* **412**, 338–341.

Rizo J & Sudhof TC (2002). Snares and Munc18 in synaptic vesicle fusion. *Nat Rev Neurosci* **3**, 641–653.

Rosenmund C, Sigler A, Augustin I, Reim K, Brose N & Rhee JS (2002). Differential control of vesicle priming and short-term plasticity by Munc13 isoforms. *Neuron* **33**, 411–424.

Rowe J, Corradi N, Malosio ML, Taverna E, Halban P, Meldolesi J & Rosa P (1999). Blockade of membrane transport and disassembly of the Golgi complex by expression of syntaxin 1A in neurosecretion-incompetent cells: prevention by rbSEC1. *J Cell Sci* **112**, 1865–1877.

Sassa T, Harada S, Ogawa H, Rand JB, Maruyama IN & Hosono R (1999). Regulation of the UNC-18-*Caenorhabditis elegans* syntaxin complex by UNC-13. *J Neuroscience* **19**, 4772–4777.

Shuang R, Zhang L, Fletcher A, Groblewski GE, Pevsner J & Stuenkel EL (1998). Regulation of Munc-18/syntaxin-1A interaction by cyclin-dependent kinase 5 in nerve endings. *J Biol Chem* **273**, 4957–4966.

Smirnova T, Fossier P, Stinnakre J, Mallet J & Baux G (1995). A syntaxin-related protein controls acetylcholine release by different mechanisms in *Aplysia*. *Neuroscience* **68**, 125–133.

Sollner TH (2003). Regulated exocytosis and SNARE function. *Mol Membrane Biol* **20**, 209–220.

Song Y, Ailenberg M & Silverman M (1998). Cloning of a novel gene in the human kidney homologous to rat munc13s: its potential role in diabetic nephropathy. *Kidney Int* **53**, 1689–1695.

Stanley EF & Mirotznik RR (1997). Cleavage of syntaxin prevents G-protein regulation of presynaptic calcium channels. *Nature* **385**, 340–343.

Tall GG, Hama H, DeWald DB & Horazdovsky BF (1999). The phosphatidylinositol 3-phosphate binding protein Vac1p interacts with a Rab GTPase and a Sec1p homologue to facilitate vesicle-mediated vacuolar protein sorting. *Mol Biol Cell* **10**, 1873–1889.

Varoqueaux F, Sigler A, Rhee JS, Brose N, Enk C, Reim K & Rosenmund C (2002). Total arrest of spontaneous and evoked synaptic transmission but normal synaptogenesis in the absence of Munc13-mediated vesicle priming. *Proc Natl Acad Sci U S A* **99**, 9037–9042.

Verhage M, de Vries KJ, Roshol H, Burbach JP, Gispen WH & Sudhof TC (1997). DOC2 proteins in rat brain: complementary distribution and proposed function as vesicular adapter proteins in early stages of secretion. *Neuron* **18**, 453–461.

Verhage M, Maia AS, Plomp JJ, Brussaard AB, Heeroma JH, Vermeer H, Toonen RF, Hammer RE, van den Berg TK, Missler M, Geuze HJ & Sudhof TC (2000). Synaptic assembly of the brain in the absence of neurotransmitter secretion. *Science* **287**, 864–869.

Vogel K, Cabaniols JP & Roche PA (2000). Targeting of SNAP-25 to membranes is mediated by its association with the target SNARE syntaxin. *J Biol Chem* **275**, 2959–2965.

Walker D & De Waard M (1998). Subunit interaction sites in voltage-dependent Ca^{2+} channels: role in channel function. *Trends Neurosci* **21**, 148–154.

Washbourne P, Cansino V, Mathews JR, Graham M, Burgoyne RD & Wilson MC (2001). Cysteine residues of SNAP-25 are required for SNARE disassembly and exocytosis, but not for membrane targeting. *Biochem J* **357**, 625–634.

Webb GC, Hoedt M, Poole LJ & Jones EW (1997). Genetic interactions between a pep7 mutation and the PEP12 and VPS45 genes: evidence for a novel SNARE component in transport between the *Saccharomyces cerevisiae* Golgi complex and endosome. *Genetics* **147**, 467–478.

Weimer RM, Richmond JE, Davis WS, Hadwiger G, Nonet ML & Jorgensen EM (2003). Defects in synaptic vesicle docking in unc-18 mutants. *Nat Neurosci* **6**, 1023–1030.

Wilson SP, Liu F, Wilson RE & Housley PR (1995). Optimization of calcium phosphate transfection for bovine chromaffin cells: relationship to calcium phosphate precipitate formation. *Anal Biochem* **226**, 212–220.

Wiser O, Bennett MK & Atlas D (1996). Functional interaction of syntaxin and SNAP-25 with voltage-sensitive L- and N-type Ca^{2+} channels. *EMBO J* **15**, 4100–4110.

Yang B, Steegmaier M, Gonzalez LC Jr & Scheller RH (2000). nSec1 binds a closed conformation of syntaxin1A. *J Cell Biol* **148**, 247–252.

Acknowledgements

We thank Dr Stephen A. Ernst (University of Michigan) for help with confocal imaging. The research was supported by a Post-doctoral Fellowship from American Heart Association 0225456Z (to S.E.G.) and by the NIH grants NS-26227 and NS-39914 (to E.L.S.).